Experimental research and clinical application of selective laser melting Ta bone plates

Dewei Zhao†,*, Baoyi Liu†, Feng Wang, Zhijie Ma, Junlei Li*

* Corresponding author. Dewei Zhao, Email: zhaodewei2016@163.com,

Junlei Li, Email: jlli11b@alum.imr.ac.cn.

†This author contributed equally to this work.

Department of Orthopaedics, Affiliated Zhongshan Hospital of Dalian University, Dalian 116001, China

Abstract

Tantalum (Ta) is widely used as a bone implant material in clinical settings. Ta is highly stable and biocompatible *in vivo*, and it is one of the metallic biomaterials with the highest affinity for bone tissue. Ta—a refractory metal—limits its application as a bone implant material. The advent of additive manufacturing (AM) technology provides a new method for fabricating Ta implants. The present study compared the microstructure, surface properties, mechanical properties, and *in vitro* and *in vivo* biological properties of selective laser melting Ta (SLM Ta), selective laser melting Ti6Al4V with a Ta coating (SLM Ti6Al4V with a Ta coating), and selective laser melting Ti6Al4V (SLM Ti6Al4V). SLM Ta has better comprehensive mechanical properties than SLM Ti6Al4V and SLM Ti6Al4V with a Ta coating. SLM Ta has anti-inflammatory activity, excellent osseointegration performance, and osteogenic bioactivity. We fabricated an SLM porous Ta bone plate through SLM and applied it for internal fixation of ulna and radius fractures. SLM porous Ta bone plate has been found to promote fracture healing. Meanwhile, the SLM porous Ta bone plate could form an integrated bone-plate structure with the bone tissue at the implanted site. Without the need for secondary surgical removal, the porous structure reduces the elastic modulus of the plate and prevents stress shielding. SLM porous Ta bone plate meets the performance requirements of an ideal bone plate and is expected to be a new generation of internal fixation bone plates for fracture.

Keywords: Ta, selective laser melting, chemical vapor deposition, osseointegration, bone plate

1. Introduction

Titanium (Ti)-based alloys and Tantalum (Ta) are widely used in orthopedic implants because of their high biocompatibility[1]. Ti-based alloys are usually forged as implant materials, whereas Ta as bone implant material is primarily porous Ta through chemical vapor deposition (CVD) or Ta coated through thermal spraying[2, 3]. Because of their lightweight and high strength, Ti-based alloys are widely used in weight-bearing implants, such as bone plates and femur stems[4]. Ta exhibits high density, rendering it unsuitable for utilization as a solid substance in the production of orthopedic implants of considerable dimensions. Instead, Ta is commonly employed in the porous form, which serves as bone defect filler or as an interface connecting implants and bone tissue[5]. Compared with Ti-based alloys, Ta has a better affinity with bone tissue. Therefore, some researchers have fabricated Ta coating on the surface of Ti-based alloys through CVD or thermal spraying to improve the alloy's bone integration performance[6].

In addition to chemical components, topological structure plays a significant role in implant performance[7]. Studies have found that scaffolds with micrometer-scaled porous structures can guide bone tissue growth, thereby repairing and regenerating bone tissue[8]. Pore size, porosity, and pore structure are crucial factors affecting bone tissue repair and regeneration of porous scaffolds[9, 10]. Conventional manufacturing methods of porous materials include mainly furnace-sintered metal powders and fibers, the space holder method, replication, and CVD[11]. However, these methods have shortcomings in the precise control of topological structure.

The emergence of additive manufacturing (AM) technology provides new technical methods for producing bone implants[12]. AM can not only realize the processing of complex porous structures but also realize the personalized customization of implants based on the anatomical characteristics of the implant site[13, 14]. Therefore, AM Ti-based alloys and Ta orthopedic implants have become popular research areas and are considered one of the future development directions for bone implants[1]. Selective laser melting (SLM) and electron beam melting (EBM) are commonly used for the fabrication of metallic orthopedic implants through AM[15]. The advantage of SLM lies in its high processing accuracy, which enables the production of implants with small pore sizes (100–1000 μm). The advantage of EBM lies in its fast printing speed, but its processing accuracy is lower than that of SLM[16].

Various clinical trials of AM Ti-based alloys and Ta orthopedic implants have compensated for the disadvantages of commercially available product specifications to meet diverse clinical needs. Moreover,

their customized shapes and unique internal porous structures confer significant advantages in anatomical structure adaptation and biomechanical properties and promote bone tissue repair and regeneration[17]. In the present study, Ti6Al4V and Ta were fabricated through SLM, and a Ta coating was fabricated on the SLM Ti6Al4V surface through CVD. As bone implant materials, the performance characteristics of SLM Ti6Al4V, SLM Ti6Al4V with a Ta coating, and SLM Ta were compared in terms of microstructure, surface energy, mechanical properties, *in vivo* and *in vitro* biocompatibility, osteogenesis, and osseointegration. This study attempted to reveal the mechanism of Ta in promoting bone repair and regeneration at the molecular biology and gene level. Additionally, it fully utilized the advantages of AM in personalized customization and develops a new type of SLM porous Ta bone plate. We applied the SLM Ta porous bone plate to fracture internal fixation, confirming its advantages in promoting fracture healing. This innovation is expected to become a new generation of biological bone plates.

2. Materials and methods

2.1 Sample preparation

Spherical Ti6Al4V (Extra Low Impurity, ELI) and Ta (purity ＞ 99.95 wt.%) powders (Stardust Technology Co., Ltd) were used to fabricate solid Ti6Al4V and Ta discs (φ20 mm × 2 mm) through SLM (Renishaw AM400, Britain). The manufacturing was performed in an argon atmosphere. Experiments were conducted with the following Ti6Al4V manufacturing parameters: a laser power of 150 W, an exposure time of 40 μs, a spot pitch of 50 μm, a layer thickness of 30 μm, and a hatch distance of 60 μm. The Ta discs were manufactured at a laser power of 260 W, with an exposure time of 100 μs, a spot pitch of 50 μm, a layer thickness of 30 μm, and a hatch distance of 65 μm. Sandblasting was performed to remove metallic powders that had adhered to the surface of the SLM Ti6Al4V and SLM Ta samples. All SLM Ti6Al4V and SLM Ta discs were polished with SiC sandpapers up to 2000 grits and then sand blasted to obtain a matte finish. Finally, the samples were ultrasonically cleaned sequentially with acetone, ethanol, and distilled water for 15 min each, then dried in warm air. The Ta coating was fabricated on the SLM Ti6Al4V through CVD to obtain SLM Ti6Al4V with a Ta coating based on previously reported parameters[18].

2.2 Material characterization

The surface morphology of various samples was observed using a scanning electron microscope (SEM), and the surface element composition of the samples was analyzed using EDS. The phase

composition of the samples was characterized using XRD. The surface energy of different samples was characterized using the contact angle test. Approximately 10 μL of ultra-pure water and diiodomethane was added to the surface of each sample group; the contact angle of ultra-pure water and diiodomethane on the sample surface was measured; the surface energy of different samples was calculated using the following Equation [1]:

$$\gamma_L(1+\cos\theta) = 2\left((\gamma_L^d\gamma_S^d)^{1/2} + \left(\gamma_L^p\gamma_S^p\right)^{1/2}\right)$$

The surface roughness of SLM Ti6Al4V, SLM Ti6Al4V with a Ta coating, and SLM Ta was characterized using laser confocal microscopy.

Five tensile samples of SLM Ti6Al4V, SLM Ta, and SLM Ti6Al4V with a Ta coating were tested to determine mechanical properties. The tensile samples (30 mm in gauge length, 6 mm in width, and 3 mm in thickness) of SLM Ti6Al4V and SLM Ta were built on the substrate using previously described parameters. The tensile samples of SLM Ti6Al4V with a Ta coating were fabricated using CVD by coating Ta on the tensile samples of SLM Ti6Al4V. Tensile tests were performed at a strain rate of 1 mm/min. The displacements were measured using an extensometer with a gauge length of 25 mm. The yield strength (YS) was determined by using the 0.2% strain offset method. The ultimate tensile strength (UTS) was calculated by dividing the maximum force during the tensile test by the cross-sectional area of the parallel section of the sample. YS, UTS and the elongation to failure (elongation) were calculated based on the average of five tests.

2.3 Cell Culture

Mouse calvaria-derived osteogenic cells (MC3T3-E1) were obtained from the Chinese Academy of Sciences Cell Bank. The cells were cultured in complete medium (α-MEM medium supplemental with 10% fetal bovine serum, 100 U/mL penicillin, and 100 μg/mL streptomycin) in a humidified incubator at 37 °C with 5% CO_2. The medium was replaced every 2 days.

2.3.1 Cell Proliferation and Morphology

Cell count kit-8 (CCK-8, Dojindo, Japan) was used to characterize cell proliferation on SLM Ti6Al4V, SLM Ta, and SLM Ti6Al4V with a Ta coating (10 mm in diameter and 1 mm in thickness). The MC3T3-E1 cells were seeded on the samples (SLM Ti6Al4V, SLM Ti6Al4V with a Ta coating, and SLM Ta) at a density of 5×10^4/well in 48-well culture plates. At 1, 4, and 7 days, a 10% CCK-8 solution-containing medium was added into the well and incubated at 37 ℃ for 2 h. Then, 100 μL of the reaction

solution was transferred to a 96-well plate, and the absorbance was measured at 450 nm with a microplate reader.

At 1, 4, and 7 days of culture, cell viability on the surfaces of SLM Ti6Al4V, SLM Ti6Al4V with a Ta coating, and SLM Ta was assessed by staining living cells with Calcein AM and dead cells with Ethidium Homodimer (LIVE/DEAD cell viability kit, Dojindo, Japan). The morphology of MC3T3-E1 cells cultured on the surfaces of SLM Ti6Al4V, SLM Ti6Al4V with a Ta coating, and SLM Ta was observed using confocal laser microscopy (CLSM). At each defined time point, the cells were washed thrice with PBS. To prepare samples for CLSM observation, we fixed the cells with 4% paraformaldehyde for 30 min and then permeabilized the cells with 0.1% Triton-X 100 in PBS for 5 min. After three washes with PBS, the cytoskeleton was stained with phalloidin staining solution (1:100, Yeasen) for 30 min. The cell nuclei were counterstained with 4'-6-diamidino-2-phenylindole (DAPI) for 5 min. After that, the samples were photographed using CLSM (Zeiss 9000, Germany).

2.3.2 Quantitative Real-Time PCR (RT-PCR).

The effect of SLM Ti6Al4V, SLM Ti6Al4V with a Ta coating, and SLM Ta surfaces on osteogenic differentiation of MC3T3-E1 cells was quantified using quantitative real-time polymerase chain reaction. The MC3T3-E1 cells were seeded on the samples (SLM Ti6Al4V, SLM Ti6Al4V with a Ta coating, and SLM Ta) at a density of 8×10^4/well in 6-well culture plates. After cell adhesion, the cells were cultured with osteogenic medium (complete medium supplemented with 50 mg/L ascorbic acid and 10 mM β-glycerol phosphate). The medium was refreshed every 2 days. At 14 and 21 days of culture, the expression of runt-related transcription factor-2 (Runx2), alkaline phosphatase (ALP), osteocalcin (OCN), osteopontin (OPN), and collagen type-1 (Col-1) was measured to evaluate the osteogenic differentiation of MC3T3-E1 cells.

2.4 Macrophage response to SLM Ti6Al4V, SLM Ti6Al4V with a Ta coating, and SLM Ta *in vitro*

2.4.1 Immunofluorescence staining

RAW 264.7 cells cultured on various samples for 48 h were fixed with 4% paraformaldehyde for 20 min, permeabilized for 20 min with 0.25% Triton X-100, and blocked for 1 h with 1% bovine serum albumin. Next, the cells were incubated overnight at 4 °C with primary antibodies against CD206 (Abcam) and iNOS (Abcam) at a 1:100 dilution. The cells were then incubated for 30 min with Alexa Fluor 488 conjugate or Alexa Fluor 594 conjugate secondary antibodies before being stained with 4′,6-

diamidino2-phenylindole for 5 min (DAPI). CLSM was used to visualize the stained cells (Zeiss LSM 9, Germany).

2.4.2 Flow Cytometry

The surface markers of M1 macrophages (CCR7) and M2 macrophages (CD206) were examined using flow cytometry. Passage 3 RAW 264.7 cells were isolated with 0.25% trypsin after being cultured for 48 h, collected, centrifuged at 1,000 g for 5 min, and the supernatant was discarded. The cells were then resuspended with 1×10^6 cells in 100 μL of PBS and incubated in the dark with 10 μL of APC-conjugated CCR7 (Miltenyi Biotec) and PE-conjugated CD206 (BD) simultaneously for 30 min at 4 °C. Subsequently, the cells were washed thrice with PBS and resuspended in 0.5 mL of PBS for flow cytometry analysis (FACS Canto II, BD Bioscience, San Jose, CA, USA).

2.4.3 Mouse Cytokine Array Panel

RAW 264.7 macrophages were cultured with SLM Ti6Al4V, SLM Ti6Al4V with a Ta coating, and SLM Ta for 48 h. During this assay, carefully selected duplicate capture antibodies were applied to nitrocellulose membranes. A mixture of diluted cell lysates and biotinylated detection antibodies was added and incubated with the Mouse Cytokine Array membrane. The capture antibodies were specifically bound to their cognate cytokine/detection antibody complexes, and any unbound material was washed away. The next step involved the sequential addition of Streptavidin-HRP and chemiluminescent detection reagents. The resulting light emitted at each spot on the membrane corresponded to the amount of cytokines bound.

2.5 Animal experiments

Animal experiments were approved by the Animal Care and Use Committee of Affiliated Zhongshan Hospital of Dalian University. Twelve female New Zealand Rabbits aged eight weeks (2.5 ± 0.2 kg) were obtained from Changsheng Biotechnology Co., Ltd. (Benxi, China). The rabbits were anesthetized by intramuscular injection of pentobarbital (20 mg/kg). The lateral skin of the femoral condyle was dissected, and the muscle was separated to expose the femoral condyle. The femoral condyle was drilled using a dental drill with a diameter of 4 mm and a depth of 8 mm. Twelve rabbits were randomly divided into three groups. SLM Ti6Al4V, SLM Ti6Al4V with a Ta coating, and SLM Ta rods with a diameter of 4 mm and a length of 8 mm were implanted, and then the muscle and skin were sutured successively. After six weeks, the rabbits were sacrificed to investigate the osseointegration of implants with different surfaces. All New Zealand white rabbits were killed with an intramuscular overdose of

pentobarbital. The femurs were removed and fixed in 4% paraformaldehyde solution for 7 days, dehydrated in gradually increasing alcohol concentrations (70%, 80%, 90%, 95%, and 100%), and finally embedded in methyl methacrylate . The embedded samples were sliced (approximately 100 μm in thickness) using a modified interlocked diamond saw (Leica Microtome, Wetzlar, Germany), which were ground and polished to a thickness of 50 μm for Van-Gieson (VG) staining. The VG-stained transverse histological sections were observed using an OLYMPUS microscope (CXX41, OLYMPUS, Japan) with a regular light source. The push-out force of the placed implants was measured using a universal testing machine.

2.6 Clinical trial

2.6.1 Patients

From September 2021 to February 2023, 20 limb fracture patients were selected from Affiliated Zhongshan Hospital of Dalian University. There were six patients with femoral shaft fractures, two with humeral shaft fractures, one with ankle fractures, two with ulnar and radius fractures, four with ulnar fractures, two with humeral nonunion, and three with femoral nonunion. There were 14 male and 6 female patients, with an average age of 66.8 ± 11.9 years (56–85 years). The patients signed the informed consent forms, which were approved by the ethics committee. The clinical trial was approved and supervised by the Medical Ethics Committee of the Affiliated Zhongshan Hospital of Dalian University on February, 28th (Dalian, China, approval No.2017.044).

2.6.2 Post-surgery management

The post-surgery immobilization consisted of a compressive dressing or leather traction and correction shoes. Depending on the surgeon's impression of bone quality and construct stability during surgery, the fractured body was immobilized with cast or traction for 15–30 days.

2.6.3 Clinical evaluation

Clinical results for our study were operation time and blood loss, X-rays were taken 4, 12, 24, 48 and 96 weeks after surgery to evaluate the fracture healing.

2.7 Statistical analysis

SPSS 20.0 statistics software was used for statistical analysis. These results are expressed as mean ± standard deviation. Multiple group comparisons were conducted using one-way analysis of variance (ANOVA) or two-way repeated measures ANOVAs over time as appropriate. If the difference was statistically significant, the least significant difference test method was used to compare the two groups.

A difference of $p < 0.05$ was deemed statistically significant.

3 Results

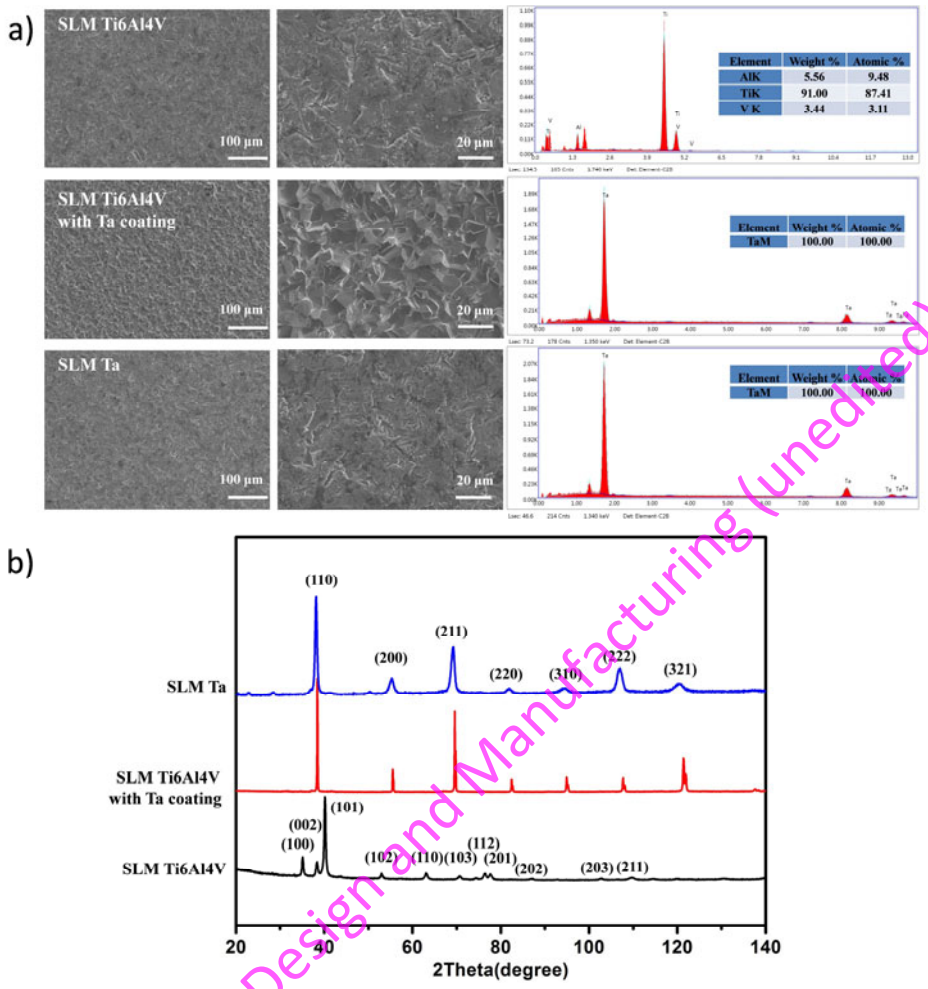

Fig. 1. (a) Surface morphology and elemental composition of SLM Ti6Al4V, SLM Ti6Al4V with a Ta coating, and SLM Ta were characterized using SEM and EDS. (b) XRD patterns of SLM Ti6Al4V, SLM Ti6Al4V with a Ta coating, and SLM Ta.

As presented in Fig. 1a, SLM Ti6Al4V and SLM Ta had similar surface morphology after sandblasting treatment, whereas the surface morphology of SLM Ti6Al4V with a Ta coating was pyramidal. EDS results revealed that the surface element composition of SLM Ti6Al4V was 91.00 wt.% Ti, 5.56 wt.% Al, and 3.44 wt.% V, consistent with the element proportion of Ti6Al4V alloy. SLM Ta and SLM Ti6Al4V with a Ta coating had the same composition of surface elements, mainly Ta. Fig. 1d shows the phase compositions—characterized using XRD—of SLM Ti6Al4V, SLM Ta, and SLM Ti6Al4V with a Ta coating. SLM Ti6Al4V was a typical α-phase hexagonal close-packed (HCP) crystal structure, whereas SLM Ta and SLM Ti6Al4V with a Ta coating possessed a body-centered cubic crystal structure.

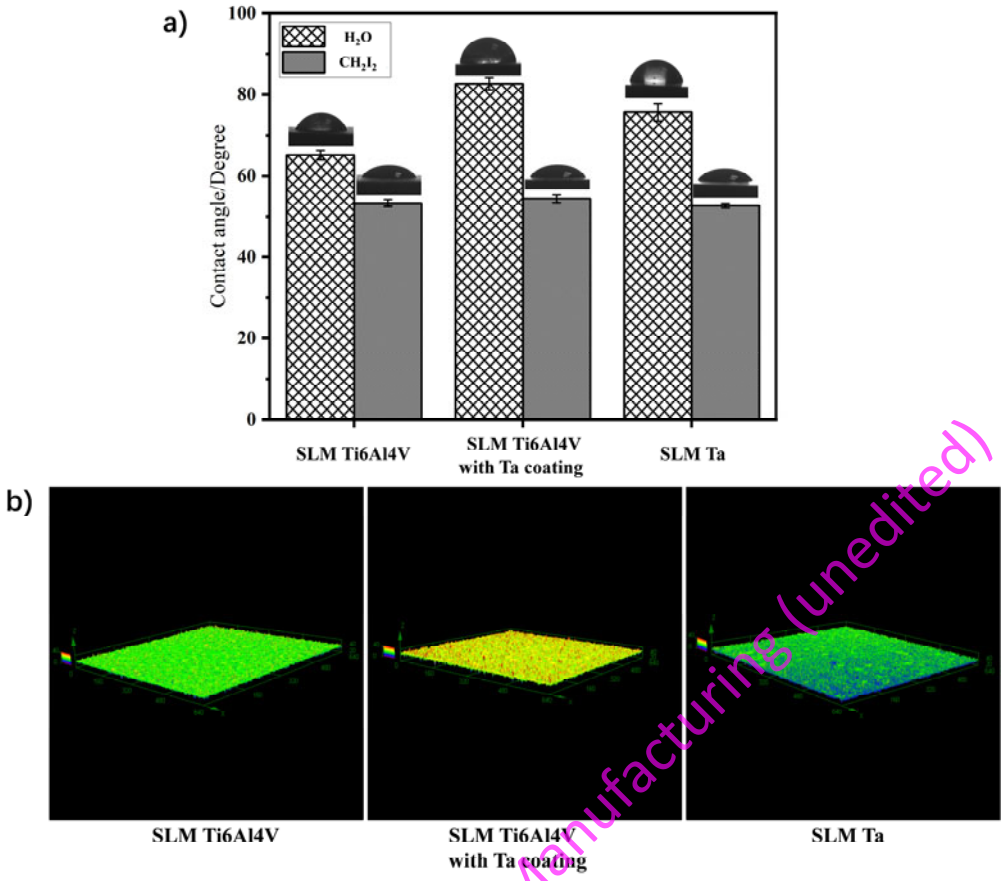

Fig. 2. (a) Contact angles of ultrapure water and diiodide on the surfaces of SLM Ti6Al4V, SLM Ti6Al4V with a Ta coating, and SLM Ta. (b) Surface CLSM images of SLM Ti6Al4V, SLM Ti6Al4V with a Ta coating, and SLM Ta.

Table 1 Surface roughness and calculated surface energy of the SLM Ti6Al4V，SLM Ti6Al4V with a Ta coating and SLM Ta

Samples	Surface roughness		Surface energy
	Ra (μm)	Rq (μm)	(mN/m)
SLM Ti6Al4V	2.000	2.651	40.6
SLM Ti6Al4V with a Ta coating	2.208	2.969	33.1
SLM Ta	2.046	2.671	35.3

The contact angle test results demonstrated that the order of hydrophilicity was SLM Ti6Al4V > SLM Ti6Al4V with a Ta coating > SLM Ta. The surface energy of different samples (Table 1) was calculated using Equation [1]. The surface energy of SLM Ti6Al4V was the highest (40.6 mN/m), followed by SLM Ta (35.3 mN/m). SLM Ti6Al4V with a Ta coating had the lowest surface energy of 33.1 mN/m.

This study detected the surface roughness of SLM Ti6Al4V, SLM Ta, and SLM Ti6Al4V with a Ta

coating using the laser confocal method (Figs. 2b–d). The surface roughness of SLM Ti6Al4V and SLM Ta after sandblasting treatment was 2 and 2.046 μm, respectively, with no significant difference. However, the roughness of SLM Ti6Al4V with a Ta coating (2.208 μm) was slightly higher than that of SLM Ti6Al4V and SLM Ta.

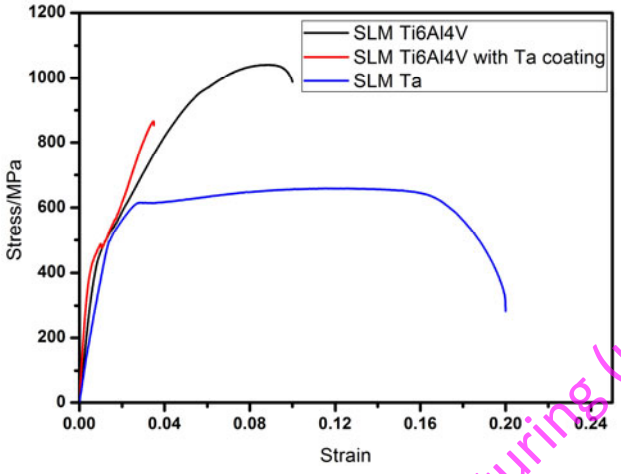

Fig. 3. Tensile stress–strain curves of SLM Ti6Al4V, SLM Ti6Al4V with a Ta coating, and SLM Ta at room temperature.

Fig. 3 illustrates the tensile curves of SLM Ti6Al4V, SLM Ti6Al4V with a Ta coating, and SLM Ta. The results of the static tensile tests are summarized in Table 2. The yield strength (YS) and ultra tensile strength (UTS) of SLM Ta were 614±22 and 659±15 MPa, respectively, and its elongation reached 20 ±0.8%. The YS and UTS of SLM Ti6Al4V were 519±21 and 1041±19 MPa, respectively, and its elongation was 9.5±0.5%. The YS and UTS of SLM Ti6Al4V with a Ta coating were 407±14 and 866 ±16 MPa, respectively, and its elongation was 3±0.2%. This finding indicates that SLM Ta has the highest plastic deformation ability, whereas SLM Ti6Al4V has the highest tensile strength. After a Ta coating was prepared on the surface of SLM Ti6Al4V through CVD, the strength and plasticity of SLM Ti6Al4V significantly decreased.

Table 2 The tensile mechanical properties of SLM Ti6Al4V, SLM Ti6Al4V with a Ta coating, and SLM Ta.

	Units	SLM Ti6Al4V	SLM Ti6Al4V with a Ta coating	SLM Ta
Yield strength, YS	MPa	519±21	407±14	614±22
Ultra tensile strength, UTS	MPa	1041±19	866±16	659±15
Elongation	%	9.5±0.5	3.0±0.2	20.0±0.8

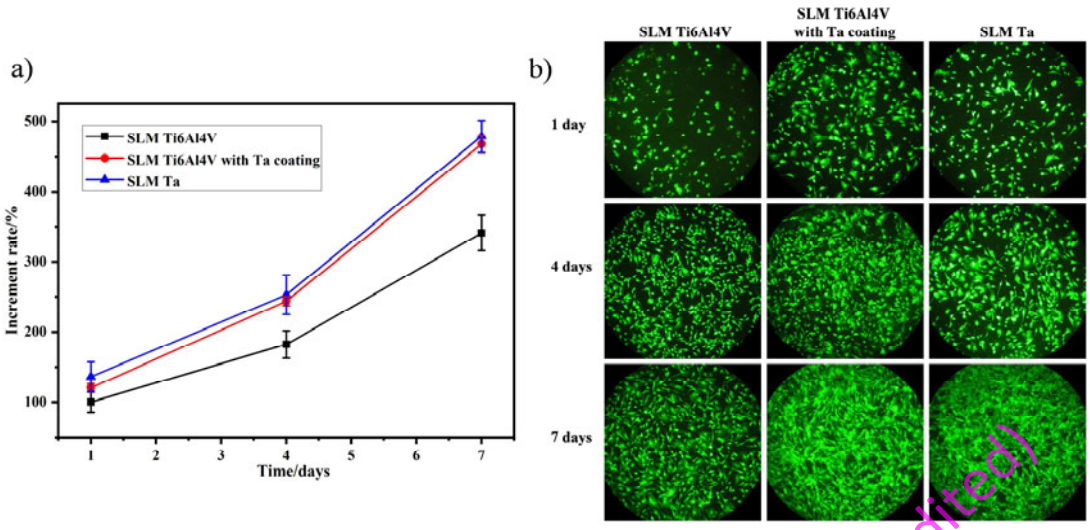

Fig. 4. (a) The proliferation of MC3T3-E1 cells on the surfaces of SLM Ti6Al4V, SLM Ta, and SLM Ti6Al4V with a Ta coating at 1, 4, and 7 days were detected using CCK-8. (b) Live-dead staining of cells cultured on the surfaces of SLM Ti6Al4V, SLM Ti6Al4V with a Ta coating, and SLM Ta at 1, 4, and 7 days.

Fig. 4a shows the CCK-8 detection of the proliferation of MC3T3-E1 cells cultured on the surfaces of SLM Ti6Al4V, SLM Ti6Al4V with a Ta coating, and SLM Ta. The number of MC3T3-E1 cells on the surfaces of all groups increased with culture time. At 1, 4, and 7 days, the number of cells on the surfaces of SLM Ti6Al4V with a Ta coating and SLM Ta was significantly higher than that of SLM Ti6Al4V, and the number of cells on the surface of SLM Ta was slightly higher than that of SLM Ti6Al4V with a Ta coating. Fig. 4b depicts the live/dead staining of MC3T3-E1 cells after culturing on the surfaces of SLM Ti6Al4V, SLM Ti6Al4V with a Ta coating, and SLM Ta at 1, 4, and 7 days. The viability of cells cultured on the surfaces of SLM Ta and SLM Ti6Al4V with a Ta coating at 1, 4, and 7 days was better than that of SLM Ti6Al4V.

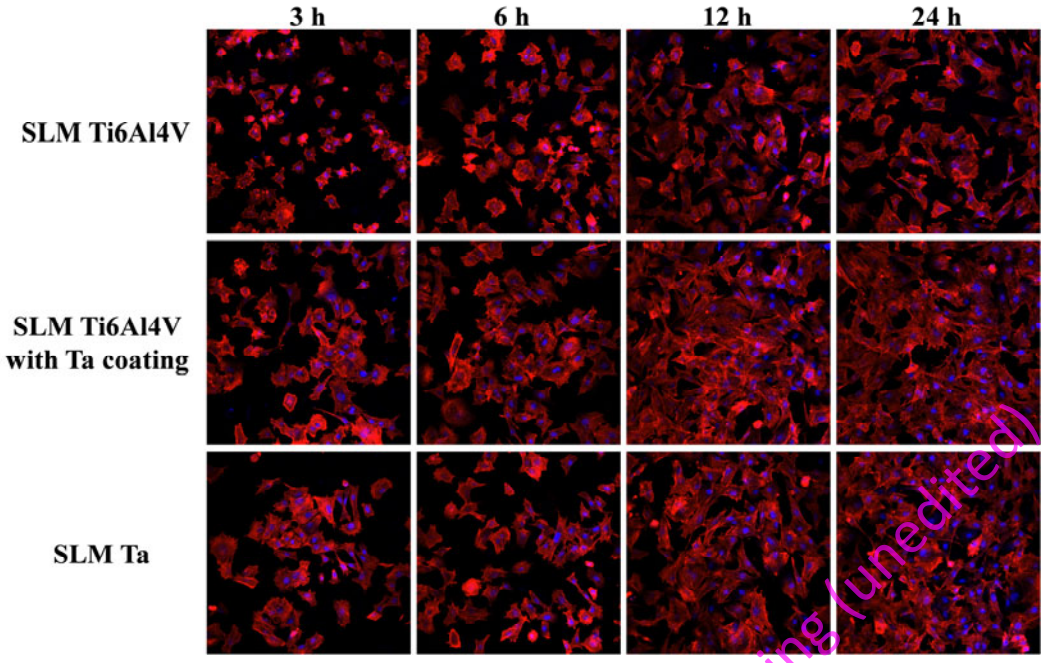

Fig. 5. Actin (red) and cell nucleus (blue) fluorescence images of MC3T3-E1 cells cultured on various surfaces at 3, 6, 12, and 24 h.

The initiated attachment of MC3T3-E1 cells on various surfaces at 3, 6, 12, and 24 h was evaluated using CLSM. As shown in the first column of Fig. 5, the cells on SLM Ta and SLM Ti6Al4V with a Ta coating promoted the maturation of focal adhesions than that on SLM Ti6Al4V. More MC3T3-E1 cells were found to have adhered on the surfaces of SLM Ti6Al4V with a Ta coating and SLM Ta. At 24 h, the cell spreading area and the number of cells on the surfaces of SLM Ti6Al4V with a Ta coating and SLM Ta were significantly larger than that of SLM Ti6Al4V, which was consistent with the results of the CCK-8 test and live/dead staining. These findings indicate that SLM Ti6Al4V with a Ta coating and SLM Ta have better cell affinity than SLM Ti6Al4V. The number and spread aera of cells on the surfaces of SLM Ti6Al4V with a Ta coating and SLM Ta did not change significantly. This finding indicates that MC3T3-E1 cells have formed stable adhesion on the surfaces of SLM Ti6Al4V with a Ta coating and SLM Ta at 3 h, whereas the number of cells and the spread area of cells on the surface of SLM Ti6Al4V has increased slightly with time. At 12 h, stable cell adhesion was formed.

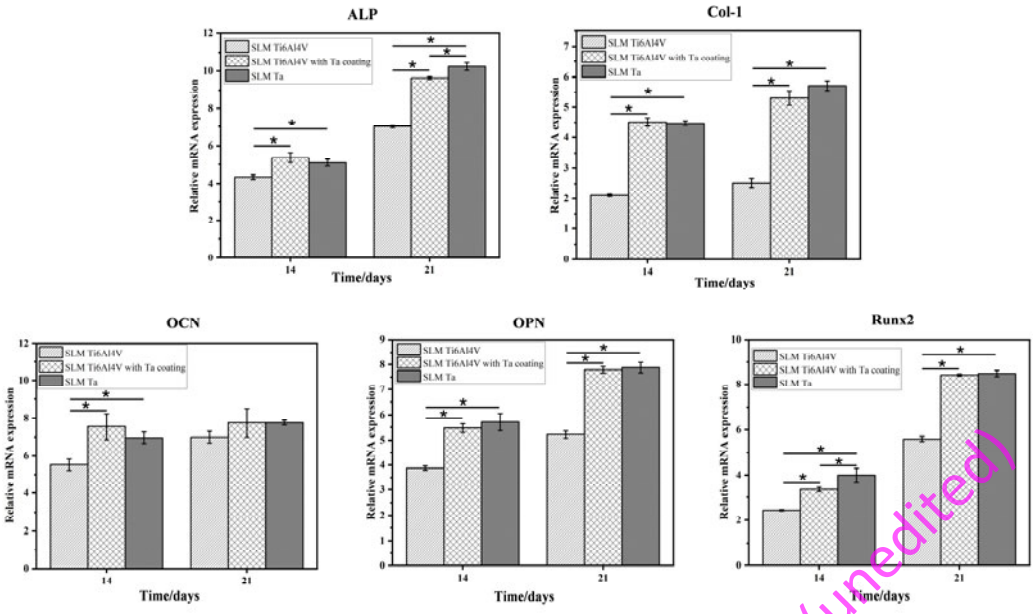

Fig. 6. Expression of ALP, Col-1, OCN, OPN, and Runx2 measured based on relative mRNA expression after 14 and 21 days of cell culture on the surfaces of SLM Ti6Al4V, SLM Ti6Al4V with a Ta coating, and SLM Ta.

As demonstrated in Fig. 6, cell differentiation was assessed using quantitative RT-PCR tests at 14 and 21 days with osteogenic markers—ALP, Col-1, OCN, OPN, and Runx2. The expression of osteogenesis-related genes in MC3T3-E1 cells cultured on the surfaces of SLM Ti6Al4V with a Ta coating and SLM Ta was significantly higher than that of SLM Ti6Al4V, proving that Ta is better than Ti in osteogenic activity. Compared with SLM Ti6Al4V with a Ta coating, the expression of the ALP gene in MC3T3-E1 cells cultured on the surface of SLM Ta was superior at 21 days. SLM Ta surface also exhibited significantly higher expression of Runx2 (at 14 days) compared with SLM Ti6Al4V with a Ta coating surface.

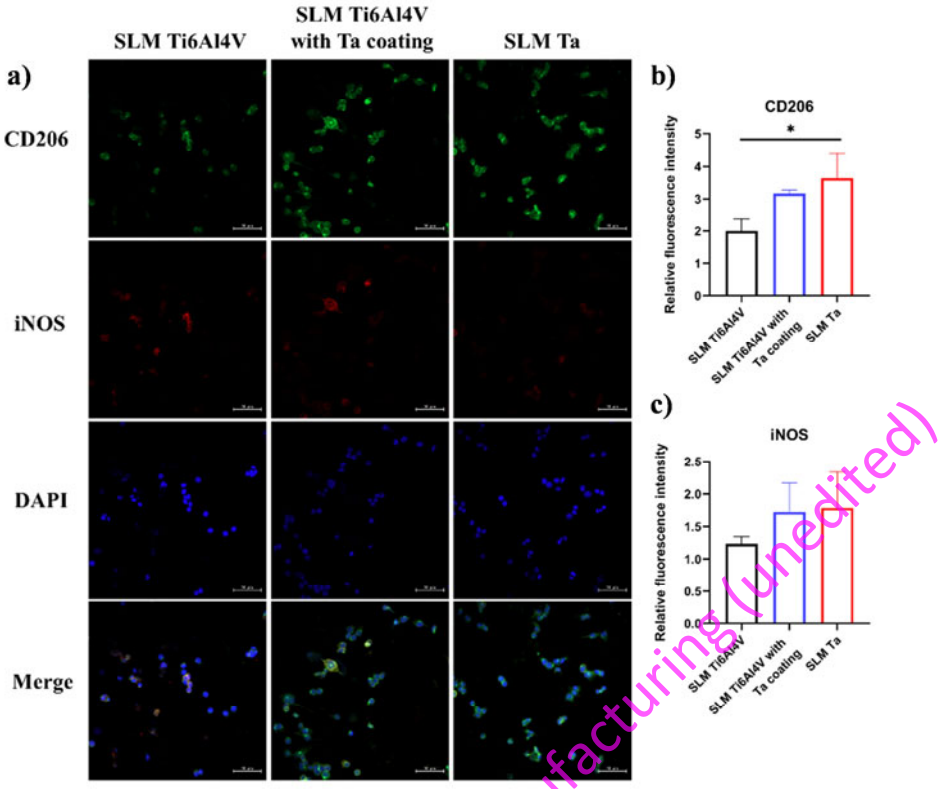

Fig. 7. (a) Fluorescence microscopy images of CD206, iNOS, and nucleic staining of macrophages on SLM Ti6Al4V, SLM Ti6Al4V with a Ta coating, and SLM Ta,

(b-c) Quantitative fluorescence intensity of CD206 and iNOS of macrophages on SLM Ti6Al4V, SLM Ti6Al4V with a Ta coating, and SLM Ta.

Immunofluorescent staining of macrophages was used to assess the effects of SLM Ti6Al4V, SLM Ti6Al4V with a Ta coating, and SLM Ta on the expression of iNOS and CD206 (Figs. 7a and b). CD206 (M2 macrophage marker) and iNOS (M1 macrophage marker) were chosen to investigate macrophage polarization. The average fluorescence intensities of iNOS of the SLM Ti6Al4V, SLM Ti6Al4V with a Ta coating, and SLM Ta groups were 1.24 ± 0.12, 1.77± 0.42 and 1.89 ± 0.51, respectively. There was no significant difference between the three groups ($p > 0.05$). Compared with the SLM Ti6Al4V group, CD206 expression in the SLM Ta group was significantly increased (3.53 ± 0.71, $p < 0.05$), indicating significantly higher anti-inflammatory response of macrophages in the SLM Ta group.

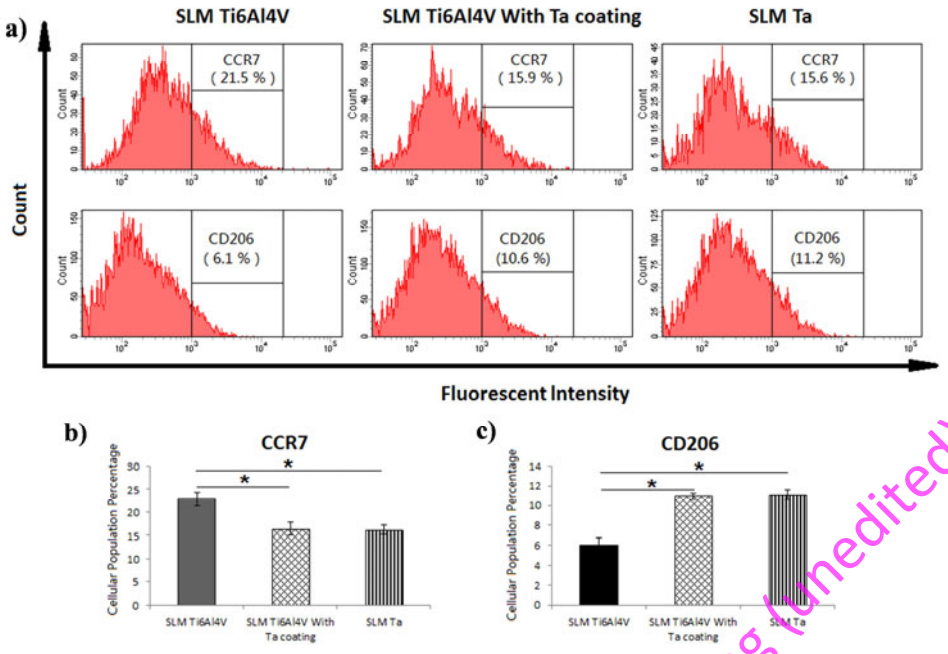

Fig. 8. (a) Polarization of macrophages cultured on SLM Ti6Al4V, SLM Ti6Al4V with a Ta coating, and SLM Ta was evaluated using flow cytometry with the expressions of CCR7 (M1) and CD206 (M2). (b-c) Quantitative fluorescence intensity of CCR7 and CD206 of macrophages cultured on SLM Ti6Al4V, SLM Ti6Al4V with a Ta coating, and SLM Ta.

CD206 is a cell-surface protein highly expressed on M2 macrophages and serves as a distinctive marker for identifying cells with M2 polarization. However, the presence of C-C chemokine receptor type 7 (CCR7) on a macrophage surface is a hallmark of the M1 phenotype, making it a useful marker for distinguishing M1 from M2 macrophages. Flow cytometry was used to evaluate macrophage polarization to confirm further the phenotype of polarized macrophages on SLM Ti6Al4V, SLM Ti6Al4V with a Ta coating, and SLM Ta. The proportion of M1 macrophages in SLM Ti6Al4V, SLM Ti6Al4V with a Ta coating, and SLM Ta was 21.5%, 15.9%, and 15.6%, respectively (Fig. 8a and b). Moreover, the proportion of M2 macrophages was 6.1% in the SLM Ti6Al4V group but higher in SLM Ti6Al4V with a Ta coating (10.9%) and SLM Ta (11.2%). These findings suggest that Ta may induce a lower immune inflammatory reaction and rejection after transplantation than Ti6Al4V and may be more conducive to tissue repair facilitated by M2 macrophages. Therefore, compared with SLM Ti6Al4V, SLM Ti6Al4V with a Ta coating and SLM Ta may offer advantages for tissue repair, owing to their potential to promote M2 macrophage-mediated healing and reduce immune-inflammatory responses.

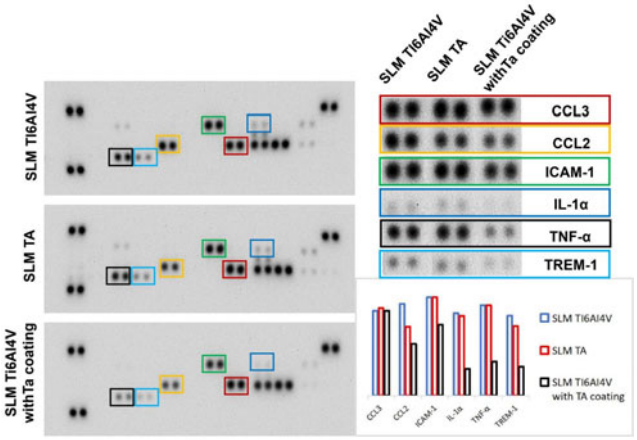

Fig. 9. Protein expression levels of inflammatory cytokines in macrophages cultured on SLM Ti6Al4V, SLM Ta, and SLM Ti6Al4V with a Ta coating.

As displayed in Fig. 9, the protein expression levels of macrophages cultured on different materials were detected using Mouse Cytokine Array Panel A. Gray value analysis revealed no significant difference in the protein expression levels of inflammatory chemokines CCL3, IL-1α, TNF-α and cell adhesion molecule ICAM-1 in macrophages between SLM Ti6Al4V and SLM Ta, whereas the protein expression levels of CCl2 and TREM-1 were significantly different. Compared with macrophages cultured in SLM Ta, macrophages cultured in SLM Ti6Al4V showed significantly increased expression levels of some pro-inflammatory factors. This finding suggests that macrophages cultured on SLM Ta exhibit a relatively weak tendency to inflammatory responses. Compared with the other two groups, the protein expression levels of macrophage inflammatory chemokines CCL2, IL-1α, TNF-α, and cell adhesion molecule-1 were significantly different in the SLM Ti6Al4V with a Ta coating group. This finding indicates that macrophages cultured on SLM Ti6Al4V with a Ta coating exhibit a significantly attenuated inflammatory response tendency.

To understand how SLM Ta and SLM Ti6Al4V activate macrophage polarization, we performed a transcriptomic analysis of macrophages cultured on different samples. The Pearson correlation between samples was used to assess sample stability through correlation analysis. Most correlation coefficients were within acceptable ranges ($R2 > 0.93$; Fig. S1). Transcriptomic analysis revealed the number of differentially expressed genes between two groups with adjacent scales (SLM Ta versus SLM Ti6Al4V, SLM Ta versus SLM Ti6Al4V with a Ta coating, SLM Ti6Al4V with a Ta coating versus SLM Ti6Al4V). Volcano plots (Fig. S2) revealed significant variation in gene expression, with 1818 genes upregulated and 1560 genes downregulated for SLM Ta versus SLM Ti6Al4V, with 1818 genes upregulated and 1560

genes downregulated for SLM Ta versus SLM Ti6Al4V with a Ta coating, and with 1818 genes upregulated and 1560 genes downregulated for SLM Ti6Al4V with a Ta coating versus SLM Ti6Al4V. These differential gene expressions are shown in the resulting heatmap (Fig. S3). Next, the differentially expressed genes between SLM Ta versus SLM Ti6Al4V were focused on undergoing gene ontology analysis. All differential genes were assessed in terms of biological process (BP), molecular function (MF), and cellular component (CC). The top 30 enriched terms of SLM Ta versus SLM Ti6Al4V are revealed in Fig. S4a. Then, KEGG pathway analysis was performed to identify the underlying signaling pathways. The top 20 enriched terms of SLM Ta versus SLM Ti6Al4V were identified using KEGG pathway analysis (Fig. S4b). We found that the TNF and chemokine signaling pathways downregulated in the SLM Ta group. In the TNF signaling pathway, the expression of TNF-α and CXCL2 genes was significantly downregulated, consistent with the results of cytokine array analysis.

Osteointegration property

SLM Ti6Al4V, SLM Ti6Al4V with a Ta coating, and SLM Ta rods were implanted into the femoral condyle of rabbits. The osseointegration properties of various samples were observed at 6 weeks.

A direct bone-implant contact (BIC) was formed around the implant surfaces of all groups (Figs. 10a–i). Significant new bone formation was observed on the surface of SLM Ti6Al4V, indicating that SLM Ti6Al4V had good biocompatibility. The trabecular bone tissues grown on the surfaces of SLM Ti6Al4V with a Ta coating and SLM Ta were thicker and stronger. In particular, the bone tissue on the SLM Ta surface was closely attached to the SLM Ta surface, and the volume of new bone was the largest. The BIC percentage and the peri-implant bone area are two crucial factors contributing to the quality of osseointegration. The BIC and the area of new bone in different groups existed in the following sequence: SLM Ta ＞ SLM Ti6Al4V with a Ta coating ＞ SLM Ti6Al4V. The BIC values in SLM Ta, SLM Ti6Al4V with a Ta coating, and SLM Ti6Al4V were 71%, 58%, and 42%, respectively, demonstrating that SLM Ta possesses the best osteoconductive ability *in vivo*.

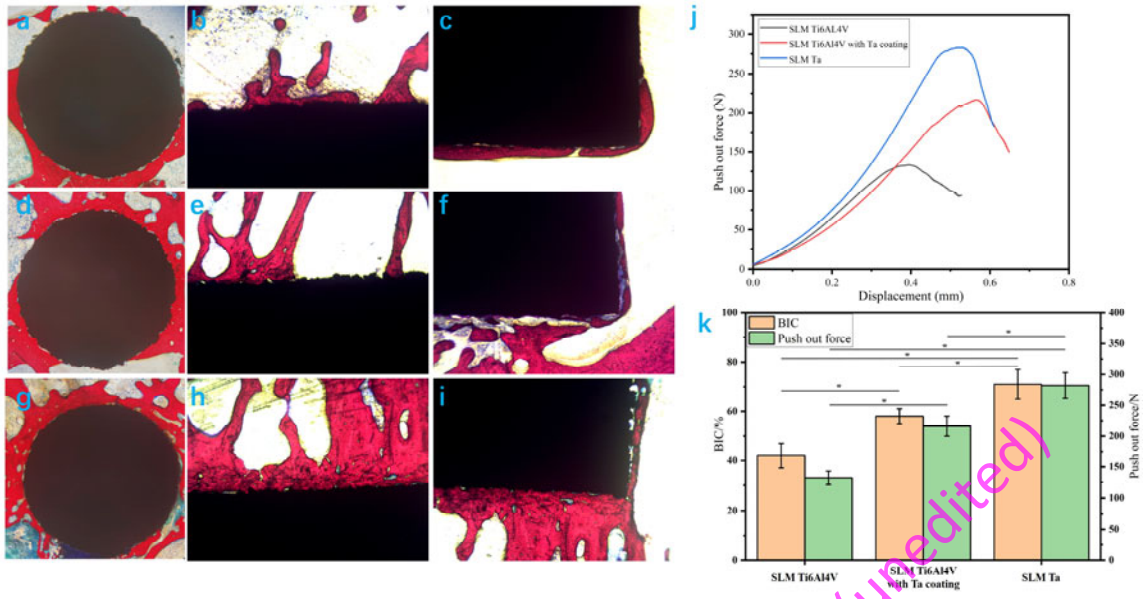

Fig. 10. The typical light microscopic images of the VG-stained histological sections of the SLM Ti6Al4V (a-c), SLM Ti6Al4V with a Ta coating (d-f), and SLM Ta (g-i) rods at 6 weeks post-surgery. (j) Load-displacement curves of SLM Ti6Al4V, SLM Ti6Al4V with a Ta coating, and SLM Ta. (k) The average BIC and push-out forces of the SLM Ti6Al4V, SLM Ti6Al4V with a Ta coating, and SLM Ta rods at 6 weeks post-surgery (*$p < 0.05$).

To evaluate the long-term bonding between the implant and bone tissue, we studied the push-out forces for the implants (Figs. 10j and k). The SLM Ti6Al4V group had the least amount of remodeled bone around the implants, with the lowest push-out force (132 N). The push-out forces of SLM Ta and SLM Ti6Al4V with a Ta coating significantly improved to 216 and 282 N, respectively, significantly higher than that of SLM Ti6Al4V ($p < 0.05$).

Pre-surgery results

Our study included 20 patients. There was no significant difference in patient characteristics. Each patient's injury and treatment were noted; all baseline characteristics were balanced.

Surgery outcomes and functional results

The fractures healed in all patients, and there were no cases of fixation failure or abnormal healing. The average time of surgery was 56.00 ± 2.65 min. The average blood loss was 145.6 ± 46.25 mL.

The mean follow-up period was 13.43 ± 6.83 months (6–24 months). The SLM Ta plate healing time was 12.47 ± 0.63 months. In the regular follow-up period, X-rays were taken at 4, 12, 24, 48, and 96 weeks post-surgery.

Clinical cases analysis

We observed the clinical effect of the SLM Ta plate through two typical limb internal fixation cases. Case 1 involved a patient with a femur nonunion (Figs. 11a–c). The X-ray taken before the surgery showed that the intramedullary nail was removed and replaced with an SLM Ta plate during the surgery. The fracture line appeared blurred at 2 months post-surgery and completely disappeared at 3 and 6 months post-surgery, indicating that the fracture had fully healed. Case 2 involved a 50-year-old female with a humeral nonunion who was treated with SLM Ta plate fixation(Figs. 11d-e). The fracture line disappeared and bone healed at 3 and 6 months post-surgery (Fig. 11f).

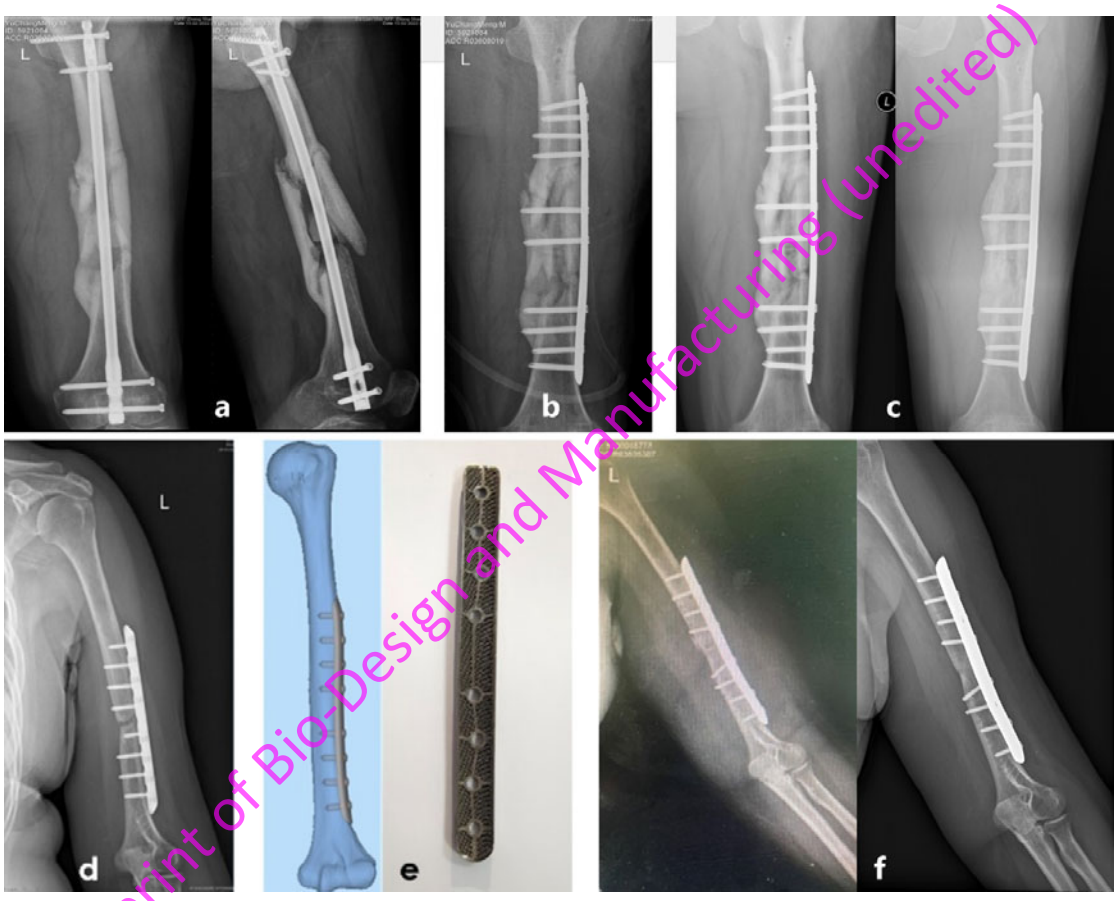

Fig. 11. Clinical data analysis. (a-c) Case 1: femur nonunion treated with SLM Ta plate fixation, which healed 12 weeks post-surgery. (a) Pre-surgery X-ray images, (b) post-surgery X-ray image, and (c) 3 and 6 months post-surgery X-ray, wherein the fracture line disappeared. (d-f) Case 2: (d) humeral nonunion in a 50-year-old female treated with SLM Ta plate fixation, (e) design and physical drawings, and (f) 3 and 6 months post-surgery X-ray, wherein the fracture line disappeared.

4 Discussion

Ti-based metallic materials and CVD porous Ta have been widely used as bone implant materials in clinical settings[6, 19]. The emergence of AM technology provides a new processing technology for

producing bone implant products. AM technology has unique advantages in making customized orthopedic implants and implants with complex porous structures. Several AM Ti6Al4V orthopedic implants have obtained registration certificates in their home countries, and a series of clinical transformations have been implemented. Most related implant products have shown good biosafety and improved clinical efficacy[16]. Compared with Ti-based metallic materials, Ta exhibited better biocompatibility and affinity with bone tissue[20, 21]. Therefore, we considered the development of Ta orthopedic implants through AM and observed their clinical performance.

The present study first compared the performance of SLM Ti6Al4V, SLM Ti6Al4V with a Ta coating, and SLM Ta as bone implantation materials. CVD-produced porous Ta has unique surface morphology and high surface roughness. To eliminate the influence of surface roughness, we increased the surface roughness of SLM Ti6Al4V and SLM Ta through sandblasting. Thus, SLM Ti6Al4V, SLM Ti6Al4V with a Ta coating, and SLM Ta exhibited similar surface roughness. Studies have mentioned that Ta has a better affinity with osteoblasts and stem cells because of its higher surface energy[20]. However, our results demonstrated that the surface energy of Ta coated through CVD and AM is lower than that of Ti6Al4V. Therefore, surface energy might not be the main factor affecting the affinity between Ta and bone tissue.

The tensile curves revealed that the tensile strength of SLM Ta was about half of that of SLM Ti6Al4V, and the elongation of SLM Ta could reach more than twice that of SLM Ti6Al4V. The mechanical properties and elongation of SLM Ti6Al4V with a Ta coating were significantly decreased compared with those of SLM Ti6Al4V, as the CVD temperature of Ta coating was 1050 ℃. At this temperature, the grain size of SLM Ti6Al4V grew significantly, weakening the grain boundary strengthening. Meanwhile, SLM Ta possessed a body-centered cubic crystal structure, whereas SLM Ti6AL4V and SLM Ti6AL4V with a Ta coating had an HCP structure. SLM Ta had more slip systems; therefore, its plastic deformation ability was significantly better than SLM Ti6AL4V and SLM Ti6AL4V with a Ta coating. The CVD temperature was higher than the annealing temperature of SLM Ti6Al4V, and the deposition time was approximately 2 h. In this condition, the grain size of SLM Ti6Al4V grew significantly, so the plastic deformation ability of SLM Ti6Al4V with a Ta coating was also significantly decreased, characterized by brittle fracture. Among all Ti-based metallic materials, β-phase Ti alloy has a body-centered cubic structure. Through alloy design or an appropriate heat treatment process to transform Ti alloy into β-phase, the plastic deformation ability of Ti alloy could be significantly improved

while maintaining the strength of Ti alloy, which is an important direction for the development of medical Ti-based metals.

In vitro cell experiments revealed that cells cultured on the surfaces of SLM Ti6Al4V with a Ta coating and SLM Ta presented better cytocompatibility. When MC3T3-E1 cells were co-cultured on the surfaces of SLM Ti6Al4V with a Ta coating and SLM Ta, the cell proliferation, adhesion, and osteogenic differentiation were better than those of SLM Ti6Al4V. SLM Ti6Al4V with a Ta coating and SLM Ta had roughness similar to SLM Ti6Al4V, and the surface energies of SLM Ti6Al4V with a Ta coating and SLM Ta were even lower than that of SLM Ti6Al4V. SLM Ta also had a similar surface morphology to SLM Ti6Al4V. Considering these factors, we speculate that the superior affinity of SLM Ti6Al4V with a Ta coating and SLM Ta to MC3T3-E1 cells might be derived from the surface chemical characteristics of Ta itself. The mechanism of enhanced osteogenesis of Ta can be explained by immunoreaction. Derek Avery et al. found that the chemical composition of the biomaterials[22] primarily drives the inflammatory response. *In vitro* macrophage studies have shown that Ta could regulate the inflammatory microenvironment and reduce the inflammatory response caused by the implant. Chronic inflammation is a leading cause of the aseptic loosening of the implant. After the implants were implanted into the human body, biological reactions occurred, including inflammatory reactions[23]. Inflammation is a protective response of the human body to injury and infection. The chemotaxis and polarization of macrophages and the release of inflammatory mediators are essential manifestations of the inflammatory response[24]. Macrophages are triggered upon contact with surrounding tissue and differentiate into various subtypes. If macrophages are polarized towards the classical activation subtype (M1), it may result in elevated levels of oxidative stress and the release of inflammatory cytokines, potentially leading to chronic inflammatory response and tissue damage, which can affect the biocompatibility of the implant. Conversely, if macrophages tend to polarize towards the alternatively activated subtype (M2), they will release anti-inflammatory factors and cytokines, thereby reducing the inflammatory response and avoiding oxidative stress[25, 26]. We demonstrated that the Ta had superior biocompatibility and caused less effect on the body, indicating a strong correlation between Ta, inflammation, and macrophage polarization[27]. Macrophage polarization is one of the key factors affecting the biocompatibility of implants. In the present study, compared with Ti6Al4V, Ta significantly increased the number of macrophages polarized to M2 type and significantly inhibited the release of inflammatory mediators, such as CCL3, CXCL2, TNF-α, and ICAM-1, from macrophages. CCL3 and CXCL2 are inflammatory

mediators that play an important role in the inflammatory process. They can recruit and activate inflammatory cells and promote inflammatory reactions[28]. TNF-α is a cytokine that can induce the aggregation and proliferation of inflammatory cells and promote inflammatory reactions[29]. ICAM-1 is an adhesion molecule that promotes the adhesion and migration of inflammatory cells. During the inflammation process, the expression of ICAM-1 is upregulated, thus increasing the possibility of inflammatory cells gathering at the site of inflammation[30]. Hence, inflammation is linked to CCL3, CXCL2, TNF-α, and ICAM-1, as these molecules can contribute to the inflammatory process in diverse ways, thereby influencing the onset and progression of inflammation.

The TNF signaling pathway can activate macrophages to produce CXCL2, thereby attracting monocytes and other immune cells into the inflammatory site and participating in the occurrence and development of the inflammatory response. Furthermore, TNF can activate various inflammatory response genes via the NF-κB pathway, thereby enhancing the ability of macrophages to respond to exogenous stimuli and further polarizing them into M1 macrophages. After the polarization of M1 macrophages, TNF can maintain their polarization and further promote the activation of M1 macrophages and the occurrence and maintenance of inflammatory response[31]. In the chemokine signaling pathway, the expression of CCL3 and CXCL2 genes was significantly downregulated, consistent with the results of cytokine array analysis. Two chemokines, CCL3 and CXCL2, also play an important role in macrophage polarization and inflammatory response. For instance, CCL3 was found to induce macrophage polarization toward M1 macrophages. After macrophages are polarized into M1 macrophages, CCL3 can activate various inflammatory responses and apoptosis-related signaling pathways[32]. CXCL2 can lead to the polarization of macrophages to M1 macrophages by activating the MyD88/TRIF pathway and regulating inflammatory response[33].

Besides, we found that the TNF and Chemokine signaling pathways of macrophages were significantly downregulated in SLM Ti6Al4V with a Ta coating and SLM Ta compared with SLM Ti6Al4V. This downregulation is essential in inhibiting other immune cells from aggregating at inflammatory sites and reducing inflammatory function activation of immune cells. These findings indicate that Ta exhibits lower immunogenicity and higher M2 polarization induction of macrophages. The immune affinity properties of Ta-based implants may contribute to their *in vivo* biocompatibility and osseointegration.

The results of the cell experiments showed that Ta was superior to Ti6Al4V in terms of anti-

inflammatory properties, biocompatibility, and osteogenic bioactivity. Therefore, the osseointegration properties of SLM Ta and SLM Ti6Al4V with a Ta coating were superior to SLM Ti6Al4V. At the same time, we also found that SLM Ta had better bone integration performance than SLM Ti6Al4V with a Ta coating. The reason for this result is that the samples of the in vitro cell experiment were all subjected to wire-cut, sanding and sandblasting treatment, and the samples of each group had similar surface roughness, in which case the properties of the material itself had a major influence on the cell behavior. For the samples used in animal experiments, the samples are too small to be polished. So the roughness of the samples was higher than that of the cell experimental group, while the surface roughness of SLM Ti6Al4V was significantly reduced after Ta coating treatment, and the rough surface was conducive to the formation of better osseointegration between the implant and bone tissue. Therefore, the BIC and push out force of SLM-Ta were superior to those of SLM Ti6Al4V with a Ta coating.

SLM Ta has excellent comprehensive mechanical properties and better biological properties to promote osseointegration and osteogenesis, so the present study attempted to clinical translation of SLM Ta. Therefore, we designed a porous Ta plate for fracture fixation. The porous Ta bone plates were fabricated through SLM. According to the anatomical structure of the fracture site, the shape of the bone plate was personalized to fit the bone tissue of the implant site perfectly. Furthermore, the porous structure of the bone plate was conducive to reducing the stress shielding of the bone plate. The growth of new bone tissue in porous Ta allows the plate to grow together with the bone tissue at the implantation site, thereby avoiding the risk of plate loosening. In the present study, an SLM porous Ta plate was used for the internal fixation of femur and humeral fractures, and the fracture healing time was significantly decreased. The 3 and 6 months post-surgery X-ray fracture healed completely. The SLM porous Ta plate grew together with the bone tissue at the implantation site, resulting in a bone-plate integration structure that did not require a second surgery to remove. According to the design concept of the ideal plate, the plate should not only provide stable mechanical fixation for the fracture ends but also have the characteristics of no stress shielding, accelerate fracture healing, and not need a second surgery[4]. Therefore, the characteristics of the SLM Ta plate developed in the present study align with the design concept of an ideal bone plate, which is expected to be more widely used in clinical practice.

Tantalum, as an orthopedic implant material, has shown excellent bone-promoting biological properties. However, its high density remains the main limitation that restricts the widespread clinical application of tantalum bone implants. A recent study has also demonstrated that using 100% Ta is

unnecessary. Similar biocompatibility can be achieved by incorporating 10 to 25% tantalum in titanium through alloy design using additive manufacturing (AM)[34]. Therefore, utilizing Ta as an alloying element to develop new orthopedic implant materials may be a potential direction in the future.

5 Conclusion

After sandblasting, SLM Ta and SLM Ti6Al4V have similar surface roughness as CVD Ta coatings. Although the surface energy of SLM Ta and CVD Ta coatings was lower than that of SLM Ti6Al4V, the proliferation, adhesion, and differentiation of MC3T3-E1 cells on the surfaces of SLM Ta and CVD Ta coating were better than those of SLM Ti6Al4V. The results of macrophage cell assays demonstrated that Ta had lower immunogenicity and was more effective in inducing macrophage M2 polarization. *In vivo* results revealed that SLM Ta had the best osseointegration performance. *In vivo* and *in vitro* experiments verified the advantages of Ta as a bone implant material in biocompatibility and promoting osteogenic bioactivity. In light of the excellent comprehensive mechanical properties of SLM Ta, we designed an SLM porous Ta bone plate and attempted to apply SLM porous Ta bone plate to the internal fixation of ulna and radius fractures and achieved satisfactory clinical treatment effects. SLM porous Ta bone plate is expected to become a new generation of biotypic internal fixation bone plate.

Author contributions

Conceptualization, Dewei Zhao and Junlei Li; Methodology, Dewei Zhao and Junlei Li; Investigation, Junlei Li, Baoyi Liu, Feng Wang, Zhijie Ma; Writing – Original Draft, Junlei Li, Baoyi Liu; Writing – Review & Editing, all authors; Funding Acquisition, Dewei Zhao; Resources, Dewei Zhao; Supervision, Dewei Zhao, Baoyi Liu.

Acknowledgements

This work was supported by the National Natural Science Foundation of China (project No. 82172398) and LiaoNing Revitalization Talents Program (project No. XLYC2203102). We thank Home for Researchers editorial team (www.home-for-researchers.com) for language editing service.

Compliance with ethics guidelines

The authors declare that they have no competing interests.

All institutional and national guidelines for the care and use of laboratory animals were followed.

All procedures followed were in accordance with the ethicals andards of the responsible commitee on human experimentation (institutional and national) and with the Helsinki Declaration of 1975, as revised in 2008 (5). Informed consent was obtained from all patients for being included in the study.

References

1. Han Q, Wang C, Chen H, Zhao X, Wang J (2019) Porous Tantalum and Titanium in Orthopedics: A Review. ACS Biomater Sci Eng 5: 5798-5824. https://doi.org/10.1021/acsbiomaterials.9b00493

2. Geetha M, Singh AK, Asokamani R, Gogia AK (2009) Ti based biomaterials, the ultimate choice for orthopaedic implants–A review. Prog Mater Sci 54:397-425. https://doi.org/10.1016/j.pmatsci.2008.06.004

3. Carraro F, Bagno A. (2023) Tantalum as Trabecular Metal for Endosseous Implantable Applications. Biomimetics 8:49. https://doi.org/10.3390/biomimetics8010049

4. Li J, Qin L, Yang K, Ma Z, Wang Y, Cheng L, et al. (2020) Materials evolution of bone plates for internal fixation of bone fractures: A review. J Mater Sci Technol 36:190-208. https://doi.org/10.1016/j.jmst.2019.07.024

5. Gao H, Yang J, Jin X, Qu X, Zhang F, Zhang D, et al. (2021) Porous tantalum scaffolds: Fabrication, structure, properties, and orthopedic applications. Mater Des 210: 110095. https://doi.org/10.1016/j.matdes.2021.110095

6. Chen Q, Thouas GA (2015) Metallic implant biomaterials. Mat Sci Eng R 87: 1-57. https://doi.org/10.1016/j.mser.2014.10.001

7. Murphy WL, McDevitt TC, Engler AJ. (2014) Materials as stem cell regulators. Nat Mater 13:547-57. https://doi.org/10.1038/nmat3937

8. Kelly CN, Miller AT, Hollister SJ, Guldberg RE, Gall K (2018) Design and Structure-Function Characterization of 3D Printed Synthetic Porous Biomaterials for Tissue Engineering. Adv Healthc Mater 7:e1701095. https://doi.org/10.1002/adhm.201701095

9. Zhang XY, Fang G, Xing LL, Liu W, Zhou J (2018) Effect of porosity variation strategy on the performance of functionally graded Ti-6Al-4V scaffolds for bone tissue engineering. Mater Des157:523-38. https://doi.org/10.1016/j.matdes.2018.07.064

10. Chen Z, Yan X, Yin S, Liu L, Liu X, Zhao G, et al (2020) Influence of the pore size and porosity of selective laser melted Ti6Al4V ELI porous scaffold on cell proliferation, osteogenesis and bone ingrowth. Mater Sci Eng C Mater Biol Appl 106:110289. https://doi.org/10.1016/j.msec.2019.110289

11. Ryan G, Pandit A, Apatsidis DP. (2006) Fabrication methods of porous metals for use in orthopaedic applications. Biomaterials, 27:2651-70. https://doi.org/10.1016/j.biomaterials.2005.12.002

12. Davoodi E, Montazerian H, Mirhakimi AS, Zhianmanesh M, Ibhadode O, Shahabad SI, et al (2022) Additively manufactured metallic biomaterials. Bioact Mater 15:214-49. https://doi.org/10.1016/j.bioactmat.2021.12.027

13. Svetlizky D, Das M, Zheng B, Vyatskikh AL, Bose S, Bandyopadhyay A, et al (2021) Directed energy deposition (DED) additive manufacturing: Physical characteristics, defects, challenges and applications. Mater Today 49:271-95. https://doi.org/10.1016/j.mattod.2021.03.020

14. Jia Z, Xu X, Zhu D, Zheng Y (2023) Design, printing, and engineering of regenerative biomaterials for personalized bone healthcare. Prog Mater Sci 134:101072. https://doi.org/10.1016/j.pmatsci.2023.101072

15. Javaid M, Haleem A. (2018) Current status and challenges of Additive manufacturing in orthopaedics: An overview. J Clin Orthop Trauma 10:380-386. https://doi.org/10.1016/j.jcot.2018.05.008

16. Zhang XZ, Leary M, Tang HP, Song T, Qian M (2018) Selective electron beam manufactured Ti-6Al-4V lattice structures for orthopedic implant applications: Current status and outstanding challenges. Curr Opin Solid State Mater Sci. 22: 75-99. https://doi.org/10.1016/j.cossms.2018.05.002

17. Li Y, Liu H, Wang C, Yan R, Xiang L, Mu X, et al (2023) 3D printing titanium grid scaffold facilitates osteogenesis in mandibular segmental defects. NPJ Regen Med 8:38. https://doi.org/10.1038/s41536-023-00308-0

18. Liu B, Ma Z, Li J, Xie H, Wei X, Wang B, et al (2021) Experimental study of a 3D printed permanent implantable porous Ta-coated bone plate for fracture fixation. Bioact Mater 10: 269-280. https://doi.org/10.1016/j.bioactmat.2021.09.009

19. Kuncická L, Kocich R, Lowe TC (2017) Advances in metals and alloys for joint replacement. Prog Mater Sci 88:232-80. https://doi.org/10.1016/j.pmatsci.2017.04.002

20. Bandyopadhyay A, Mitra I, Shivaram A, Dasgupta N, Bose S (2019) Direct comparison of additively manufactured porous titanium and tantalum implants towards in vivo osseointegration. Addit Manuf 28:259-266. http://doi.org/10.1016/j.addma.2019.04.025

21. Balla VK, Bodhak S, Bose S, Bandyopadhyay A (2010) Porous tantalum structures for bone implants: fabrication, mechanical and in vitro biological properties. Acta Biomater 6:3349-59. https://doi.org/10.1016/j.actbio.2010.01.046

22. Avery D, Morandini L, Celt N, Bergey L, Simmons J, Martin RK, et al (2023) Immune cell response to orthopedic and craniofacial biomaterials depends on biomaterial composition. Acta Biomater 161: 285-297. https://doi.org/10.1016/j.actbio.2023.03.007

23. Gibon E, Amanatullah DF, Loi F, Pajarinen J, Nabeshima A, Yao Z, et al (2017) The biological response to orthopaedic implants for joint replacement: Part I: Metals. J Biomed Mater Res B Appl Biomater 105:2162-73. https://doi.org/10.1002/jbm.b.33734

24. Seyedizade SS, Afshari K, Bayat S, Rahmani F, Momtaz S, Rezaei N, et al (2020) Current status of M1 and M2 macrophages pathway as drug targets for inflammatory bowel disease. Arch Immunol Ther Exp 68:1-24. https://doi.org/10.1007/s00005-020-00576-4

25. D'alessio S, Correale C, Tacconi C, Gandelli A, Pietrogrande G, Vetrano S, et al (2014) VEGF-C–dependent stimulation of lymphatic function ameliorates experimental inflammatory bowel disease. J Clin Investig 124:3863-78. https://doi:10.1172/JCI72189

26. Zhu W, Yu J, Nie Y, Shi X, Liu Y, Li F, et al (2014) Disequilibrium of M1 and M2 macrophages correlates with the development of experimental inflammatory bowel diseases. Immunol Invest 43:638-52. https://doi.org/10.3109/08820139.2014.909456

27. Abaricia JO, Shah AH, Chaubal M, Hotchkiss KM, Olivares-Navarrete R (2020) Wnt signaling modulates macrophage polarization and is regulated by biomaterial surface properties. Biomaterial 243:119920. https://doi.org/10.1016/j.biomaterials.2020.119920

28. Ghafouri-Fard S, Shahir M, Taheri M, Salimi A (2021) A review on the role of chemokines in the pathogenesis of systemic lupus erythematosus. Cytokine 146:155640. https://doi.org/10.1016/j.cyto.2021.155640

29. Zelová H, Hošek J (2013) TNF-α signalling and inflammation: interactions between old acquaintances. Inflamm Res 62:641-51. https://doi.org/10.1007/s00011-013-0633-0

30. Bui TM, Wiesolek HL, Sumagin R (2020) ICAM-1: A master regulator of cellular responses in inflammation, injury resolution, and tumorigenesis. J Leukoc Biol 108:787-99. https://doi.org/10.1002/JLB.2MR0220-549R

31. Donlin LT, Jayatilleke A, Giannopoulou EG, Kalliolias GD, Ivashkiv LB (2014) Modulation of TNF-induced macrophage polarization by synovial fibroblasts. J Immunol 193: 2373-83. https://doi.org/10.4049/jimmunol.1400486

32. Yuan X, Liu W, Li Y, Chen K, Li H, Tang H, et al (2022) CCL3 aggravates intestinal damage in NEC

by promoting macrophage chemotaxis and M1 macrophage polarization. Pediatr Res 94: 119–128. https://doi.org/10.1038/s41390-022-02409-w

33. Ge S, Yang W, Chen H, Yuan Q, Liu S, Zhao Y, et al (2021) MyD88 in macrophages enhances liver fibrosis by activation of NLRP3 inflammasome in HSCs. Int J Mol Sci 22: 12413. https://doi.org/10.3390/ijms222212413

34. Mitra I, Bose S, Dernell WS, Dasgupta N, Eckstrand C, Herrick J, et al (2021) 3D Printing in alloy design to improve biocompatibility in metallic implants. Mater Today 45:20-34. https://doi.org/10.1016/j.mattod.2020.11.021